Tools and Technologies

Molecular Cancer Therapeutics

A c-Myc Activation Sensor-Based High-Throughput Drug Screening Identifies an Antineoplastic Effect of Nitazoxanide

Hua Fan-Minogue[1,5,6,7], Sandhya Bodapati[1,5,6], David Solow-Cordero[3], Alice Fan[4], Ramasamy Paulmurugan[5,6], Tarik F. Massoud[1,5,6,8], Dean W. Felsher[4], and Sanjiv S. Gambhir[1,2,5,6]

Abstract

Deregulation of c-Myc plays a central role in the tumorigenesis of many human cancers. Yet, the development of drugs regulating c-Myc activity has been challenging. To facilitate the identification of c-Myc inhibitors, we developed a molecular imaging sensor–based high-throughput screening (HTS) system. This system uses a cell-based assay to detect c-Myc activation in a HTS format, which is established from a pure clone of a stable breast cancer cell line that constitutively expresses a c-Myc activation sensor. Optimization of the assay performance in the HTS format resulted in uniform and robust signals at the baseline. Using this system, we conducted a quantitative HTS against approximately 5,000 existing bioactive compounds from five different libraries. Thirty-nine potential hits were identified, including currently known c-Myc inhibitors. There are a few among the top potent hits that are not known for anti–c-Myc activity. One of these hits is nitazoxanide, a thiazolide for treating human protozoal infections. Validation of nitazoxanide in different cancer cell lines revealed a high potency for c-Myc inhibition with IC_{50} ranging between 10 and 500 nmol/L. Oral administration of nitazoxanide in breast cancer xenograft mouse models significantly suppressed tumor growth by inhibition of c-Myc and induction of apoptosis. These findings suggest a potential of nitazoxanide to be repurposed as a new antitumor agent for inhibition of c-Myc–associated neoplasia. Our work also demonstrated the unique advantage of molecular imaging in accelerating discovery of drugs for c-Myc–targeted cancer therapy. *Mol Cancer Ther; 12(9); 1896–905. ©2013 AACR.*

Introduction

MYC was the first oncogene linked to human cancer biology and among the most deregulated genes in the cancer genome (1). Sustained activation of the c-Myc protein upregulates a cohort of target genes involved in cell cycle, proliferation, growth, metabolism, and apoptosis, which contribute to tumorigenesis in a majority of human cancers (2). Intense research on modulation of c-Myc function has shown the feasibility and benefits of c-Myc inhibition as an anticancer therapeutic strategy (3, 4).

Yet, the development of an effective therapeutic approach to target c-Myc has been challenging (5). Many attempts have been made to target c-Myc at the transcriptional level, either by inhibiting *myc* promoter activation (6–8) or destabilizing *myc* transcripts, to downregulate c-Myc. Most of these approaches have involved using antisense oligonucleotides and siRNA, which showed certain efficacy in inhibiting tumor growth but were often unstable and difficult to deliver *in vivo* (9). Most recently, bromodomain proteins were found to regulate *myc* expression through a chromatin-dependent signal transduction. Inhibition of these proteins by *de novo* small molecules resulted in downregulation of c-Myc expression and showed efficacy in animal multiple myeloma (10) and leukemia models (11). This may point to a new route to target *myc* expression using small-molecule inhibitors, yet clinical development of new drug-like molecules is often challenging. Other attempts were made to repress c-Myc activity at the protein level, either by disrupting c-Myc interaction with other factors (12, 13) or suppressing its upstream activation signaling pathway, such as mitogen-activated protein kinase (MAPK), to inhibit c-Myc activation. MAPK inhibitors have shown great results in many preclinical models (14), however, most of them have failed in clinical trials, either due to lack of therapeutic efficacy, such as for PD98059 and U0126, or poor bioavailability and high toxicity, such as for CI1040 and PD0325901 (15). Recently, atorvastatin, a family member of the Statins, was shown to reduce phosphorylation-mediated c-Myc activation by inhibiting HMG-coA reductase, and to have efficacy in different preclinical tumor models, such as lymphoma and

Authors' Affiliations: Departments of [1]Radiology, [2]Bioengineering & Materials Science and Engineering, [3]Chemical Biology, and [4]Hematology and Oncology, [5]Molecular Imaging Program at Stanford, [6]Bio-X Program, and [7]Bioinformatics Program, Stanford University School of Medicine, James H. Clark Center, Stanford, California; and [8]Department of Radiology, University of Cambridge School of Clinical Medicine, Cambridge, United Kingdom

Note: Supplementary data for this article are available at Molecular Cancer Therapeutics Online (http://mct.aacrjournals.org/).

Corresponding Author: Sanjiv S. Gambhir, Molecular Imaging Program at Stanford, Stanford University School of Medicine, 318 Campus Drive, East Wing, 1st Floor, Stanford, CA 94305-5427. Phone: 650-725-2309; Fax: 650-724-4948; E-mail: sgambhir@stanford.edu

doi: 10.1158/1535-7163.MCT-12-1243

hepatocellular carcinoma (16, 17). However, its clinical efficacy in tumor inhibition remains to be determined. To date, despite ample efforts, there have been no effective approaches to target c-Myc for cancer therapy, underscoring the continuing need for new therapeutic agents, perhaps also new approaches to accelerate development of effective c-Myc drugs.

Multimodality molecular imaging, a spectrum of imaging technologies and strategies, provides a rapid way to detect and quantify tumor response to drugs in a noninvasive and repetitive manner, and has become a key approach to accelerate drug development in both preclinical and clinical settings (18, 19). Recent development of a c-Myc activation sensor provides a way to noninvasively monitor c-Myc activity in cells and living animals (16). This sensor is based on a split luciferase complementation system, where N-terminal and C-terminal firefly luciferase fragments (NFL and CFL) were fused with a c-Myc activation motif and a GSK3β phospho-site–binding domain, respectively (16). Phosphorylation-mediated c-Myc activation induces recognition and binding of the c-Myc motif by the GSK3β domain, which brings two split firefly luciferase fragments close together to complement. The complementation of the NFL and CFL fragments results in reconstitution of firefly luciferase activity, thus c-Myc activation is detected upon the substrate addition of D-luciferin (D-Luc; Supplementary Fig. S1).

In this study, we used the c-Myc sensor to establish a cell assay and optimized it to a high-throughput screening (HTS) format. Using this assay in a quantitative HTS (qHTS) platform, we screened about 5,000 existing bioactive compounds for potential c-Myc inhibitors. Among the most potent hits was nitazoxanide, a human antiprotozoal drug. We further validated its inhibitory effect on c-Myc in different tumor cell lines and the efficacy of tumor inhibition in mouse xenograft models. Our HTS approach revealed for the first time the anti–c-Myc effect of nitazoxanide and its potential role as an antineoplastic agent. This study also demonstrates the unique role of molecular imaging in accelerating drug development for c-Myc–targeted cancer therapy.

Materials and Methods

Chemicals and drugs

PD98059 and U0126 were purchased from Cell Signaling Technology. Purified atorvastatin was purchased from Sequoia Research Products. The pure compound of nitazoxanide was purchased from Sigma. The 500 mg tablet of nitazoxanide (Generic Alinia) was purchased from Buypharma.com. The purity and quantity of the drug was validated using liquid chromatography/mass spectrometry (LC/MS). D-Luc was purchased from BIOSYNTH.

Cell culture and cell lines

All cell culture media were purchased from Invitrogen and supplemented with 10% FBS and 1% penicillin/streptomycin solution. SKBR3 (human breast adenocarcinoma) cells were cultured in McCoy's 5a medium. Osteosarcoma-derived cell line 1325 was cultured in Dulbecco's modified Eagle medium. Lymphoma cells were cultured in RPMI medium supplemented with extra 3.96×10^{-4}% of 2-mercaptoethanol (Sigma). All cells were incubated at 37°C with 5% CO_2. The SK-ST and SK-FST stable cells were established by transient transfection of the sensor system or the full-length firefly luciferase genes on a single vector, and selected with 3 μg/mL puromycin (Invitrogen). SKBR3 cell line was originally purchased from American Type Culture Collection and passaged in-house. The 1325 and lymphoma cells were provided by the laboratory of Dr. Dean Felsher from the Department of Hematology and Oncology, Stanford University, Stanford, CA. Although cell lines were not subjected to further genetic authentication, their characteristic morphologies and certain biochemical features were specifically verified. For example, overexpression of c-Myc in SKBR3 was always observed. In addition, all cell lines were tested negative for PCR evaluation for *Mycoplasma* pathogen using MycoAlert Kit (Lonza).

Western blotting

Total cell lysates were collected using 1× cell lysis buffer, as directed by the manufacturer (Cell Signaling Technology). The protein concentration was determined using the Bio-Rad DC protein assay. SDS-PAGE analysis of 50 μg of protein was transferred to Immobilon-P membrane (Millipore). Anti–phospho-c-Myc (Thr58/Ser62) and anti–c-Myc antibody (Cell Signaling Technology) were used to visualize the phospho c-Myc and c-Myc protein, respectively, as directed by the manufacturer. Anti–FLuc-HRP antibody was used to detect the firefly luciferase fragments, as directed by the manufacturer (Sigma). β-Actin protein was used as loading control and detected by anti–β-actin antibody (Sigma). Immunoblots were developed using enhanced chemiluminescence (ECL) kit (Pierce), as directed by the manufacturer. The protein level was determined by quantitation of the band intensities on Western blot analyses using the region of interest (ROI) manager of ImageJ software (Open Source).

Luciferase activity assay

Bioluminescence imaging of luciferase activity in intact cells was conducted as described previously (5). Briefly, after indicated time of treatment, culture medium was added with PBS (pH 7.0) solution of 45 μg/mL D-Luc for firefly luciferase imaging in *in vivo* imaging system (IVIS) 50 (Xenogen). Images were acquired in 2 minutes interval until reaching the peak signal. The photon output of firefly luciferase was normalized to the total protein of the cell lysates, measured by Bio-Rad DC protein assay as directed by the manufacturer (Bio-Rad).

Inhibition assay

For measuring the inhibitory effect on the sensor signal, SKBR3 stable cells, constitutively expressing the sensor system (SK-ST) or the full-length firefly luciferase (SK-FST), were treated with nitazoxanide (0, 50 nmol/L, 100 nmol/L,

200 nmol/L, 500 nmol/L, 1,000 nmol/L) for 16 hours, PD98059 (0, 10 μmol/L, 20 μmol/L, 50 μmol/L, 100 μmol/L, 200 μmol/L) for 2 hours, U0126 (0, 5 μmol/L, 10 μmol/L, 20 μmol/L, 40 μmol/L, 80 μmol/L) for 1 hour, and atorvastatin (0, 3 μmol/L, 5 μmol/L, 20 μmol/L, 50 μmol/L) for 16 hours and subjected to luciferase activity assay. For analyzing the effect on protein level, SKBR3, lymphoma, and osteosarcoma cells were treated as above and lysed for Western blotting of phospho c-Myc, c-Myc, and β-actin proteins. The IC_{50} of protein inhibition was determined using nonlinear regression-based curve fitting and a variable model of four parameters in Prism. All treatments were repeated at least three times and the error bar indicates the ±SD from the mean of all the repeats.

Bioluminescence imaging of living mice

Healthy female NU/NU mice of age 8 to 12 weeks were used (Charles River Laboratories). The Animal handling was carried out in accordance with Stanford University Animal Research Committee guidelines. Bioluminescence imaging of mouse xenografts were conducted in IVIS Spectrum (Xenogen) as described previously (20) with some modifications. Firefly luciferase imaging was acquired with D-Luc PBS solution (45 μg/μL, 100 μL) via intraperitoneal injection. A total of 5×10^6 of SK-ST or SK-FST cells were subcutaneously implanted into nude mice (nu/nu; $N = 12$ each type) as indicated to make two xenograft models. Each model was repeated three times. The mean of the three repeats and the SEM were graphed. Firefly luciferase imaging started 1 day after the implantation and continued on every other day thereafter. Three days after tumor implantation, half of the mice were gavaged twice a day with nitazoxanide 0.5% carboxymethylcellulose (CMC) solution (50 mg/mL, 100 μL) or half with 0.5% CMC solution only (100 μL). Mice were sacrificed after 27 days of treatment. Each xenograft tumor mass was completely dissected and tissue samples were collected for Western blotting of phospho c-Myc, c-Myc, and α-tubulin proteins. Three samples from each treatment and control group were collected for hematoxylin and eosin (H&E) and immunohistochemical (IHC) staining for Ki67 and caspase-3 (Histo-Tec Laboratory). At least three fields of view were examined for each stained sample. The mean of the average positive stained cells in each sample was calculated and the SEM between each sample was recorded.

Quantitative HTS of compound libraries

HTS was conducted at Stanford High-Throughput Bioscience Center (HTBC; Stanford, CA). Cells were dispensed using the Matrix WellMate (Thermo Scientific) in 100 μL culture medium into each well of the 384 white bottom plate from columns 1 to 22 (E&K Scientific) and incubated for 24 hours at 5% CO_2 and 37°C before compound addition. Hundred microliter of medium alone was added to column 23 to 24 to control for background signals. Total of 4,846 compounds from 5 different libraries, NIH Clinical Collection (NCC), Sigma LOPAC, Microsource Spectrum (MS), Biomol_ICB (BMI), and Biomol_FDA (BMF) library, were screened. All compounds are in 100% dimethyl sulfoxide (DMSO) solution and the stock concentration is 10 mmol/L in NCC and seven 2-fold titration series, 0.3125, 0.625, 1.25, 2.5, 5, 10, and 20 mmol/L, in the rest of the libraries. Approximately, 100 nL of each compound at each concentration was added directly to each well and repeated one time in columns 3 to 22 using a PinTool (V&P Scientific) on a Sciclone ALH3000 (Caliper Sciences) to achieve 1,000-fold dilution. Cells in columns 1 to 2 that were not treated with compounds were used as control for 100% activity. Twenty-four hours after compound addition, the D-Luc substrate was added using multidrop liquid dispenser and imaged using the Analyst GT (Molecular Device), with an acquisition time of 0.2 s/well. The coefficient of variation (CV) is calculated by σ/μ and the Z factor is calculated by $1 - (3\sigma_{max} + 3\sigma_{min})/|\mu_{max} - \mu_{min}|$ (μ, mean; σ, SD).

Data analysis

Curve fitting and Student t test were conducted using Excel (Microsoft 2008) and Prism. Data are presented as described in each experimental method. Generally, for *in cellulo* experiments, the data point on the graph is the mean between repeated measurements, and the error bar is the SD from the mean. For *in vivo* experiments, the data point is the mean between repeated treatment experiments and the error bar is the SEM. $P < 0.05$ was used as cutoff point for statistical significance.

Results

Development of a HTS system using a c-Myc activation sensor-based cell assay

A recent bioluminescence imaging sensor that can noninvasively detect the phosphorylation-mediated activation of c-Myc (Supplementary Fig. S1), provides a rapid and quantitative approach to measure c-Myc activity upon drug inhibition in an intact biologic system (21). To facilitate the drug development against c-Myc, we constructed a stable cell line constitutively expressing this c-Myc sensor, developed it into a cell assay, and optimized it in a HTS format. The sensor was first transfected into SKBR3 cells, a breast cancer cell line with overexpression of the c-Myc protein. A single pure clone of SKBR3 cells with stable and relatively high sensor signal was selected for the development of a cell assay that can detect c-Myc activation in a HTS format. To determine the optimal cell concentration for the detection assay, 6,000 to 18,000 sensor stable cells (SK-ST), in increments of 2,000, were each plated in 5 consecutive columns of 384-well plates in 100 μL/well and incubated for 24 hours before imaging. To measure the performance of the assay, the percentage of CV (CV%) for comparing variation between concentrations and the Z factor for assessing the quality of entire screen were calculated. Although the sensor signals were correlated well with different cell concentrations ($R^2 = 0.99$; Supplementary Fig. S2A and S2B), the CV of the sensor signals decreased from 32% at 6,000 cells per well to 7% at 12,000 cells per well and increased back to about 26%

at 14,000 cells per well and above (Supplementary Fig. S2C). Because lower CV% indicates less intragroup variation, these results suggest that a cell concentration of 12,000 cells/100 μL/well in a 384-well plate were optimal to achieve low signal variation between wells.

To obtain a higher signal-to-noise ratio, we evaluated the substrate concentration effect on the intensity and variability of the assay signal. Of note, 45 mg/mL stock substrate, D-Luc, in 0.02, 0.01, 0.005, 0.002, and 0.001 dilution ratios, was added directly to each well of 12,000 cells. Of note, 0.02 (50-fold) dilution ratio, which results in 900 μg/mL D-Luc, yielded the highest signal, 2.5E + 05 p/s/cm^2/sr, and the lowest CV%, 6.2% (Supplementary Fig. S3A and S3B). Dilution ratios higher than 0.02 resulted in cell toxicity and dramatic color change of the medium. We also found that, due to the kinetics of the enzyme–substrate reaction, the assay signal was unstable at the early time points after substrate addition. The average signal intensity increased and reached a plateau at 10 minutes after D-Luc addition and the CV% decreased from about 30% at 2 minutes to less than 10% at 10 minutes after D-Luc addition in 3 separate experiments (Supplementary Fig. S3C and S3D). These results suggested that the optimal substrate concentration is 900 μg/mL D-Luc and the optimal assay time is 10 minutes after substrate addition.

To validate the quality of the assay under optimal conditions at the baseline, 6 384-well plates were seeded with 12,000 cells/100 μL/well in the first to the 22nd columns and 100 μL medium alone in the last 2 columns as the blank control. The assay signal was measured 10 minutes after addition of 900 μg/mL D-Luc. The CV% and *Z* factor (22) ranged between 11.4% to 9.3% and 0.67 to 0.72, respectively (Supplementary Fig. S4). These data showed the uniformity and robustness of the assay in a HTS format.

A quantitative HTS for inhibitors of c-Myc activation

Using the optimized sensor-based cell assay, we conducted a qHTS against 4,846 existing bioactive compounds from 5 different libraries, the NCC, Sigma LOPAC, MS, BMI, and BMF (Fig. 1). The NCC library has more than 400 drugs that have been used in clinic or clinical trials. The LOPAC library from Sigma-Aldrich has close to 1,300 compounds with proven pharmacologic activities in a variety of cell signaling and neuroscience fields (23). The MS, BMI, and BMF libraries have more than 3,000 compounds, which also include about 800 natural products. In a qHTS platform, compounds were tested at seven different concentrations simultaneously, 0.3125, 0.625, 1.25, 2.5, 5, 10, and 20 μmol/L, except the NCC drugs, which were tested at a single concentration of 10 μmol/L. The initial hits of 337 compounds, about 10% of the total, were revealed to have a minimum of 30% inhibition at 10 μmol/L. To filter out cytotoxic agents and known luciferase inhibitors, we compared our screening results with those in the MDL Assay Explorer database, which contains dose response profiles of screenings for antiproliferation and luciferase inhibition against the same libraries. Finally, 39 compounds, about 1% of the total, were identified as potential clean hits (Fig. 1). These potential hits (2 from the NCC library, 3 from the LOPAC library, and 34 from the combined MS, BMI, and BMF libraries) are from many compound classes (Supplementary Fig. S5). The IC_{50} of the potential hits, except those from the NCC library, ranged from 1.18 to 42.8 μmol/L (Supplementary Figs. S6 and S7). Among the top hits with high efficacy, there are known inhibitors of kinases upstream of c-Myc, such as calphostin C, a protein kinase C (PKC)–specific inhibitor (24, 25). We also see drugs that are not previously described to have anti–c-Myc activity, such as nitazoxanide, an antiparasitic drug; 4-chloromercuribenzoic acid (pCMB), a standard cysteine protease inhibitor; and fludarabine phosphate, a purine analog acting as an antimetabolite for chemotherapy (Supplementary Fig. S8). Nitazoxanide is especially interesting because it is a widely used off-label drug and well tolerated with very few side effects (26). In this study, we chose nitazoxanide to further validate our sensor-based HTS system.

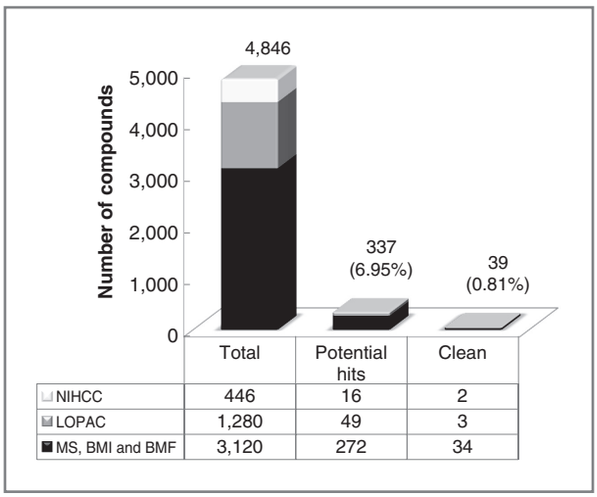

Figure 1. Summary of the HTS results. The contribution of each library to the total screened compounds, the potential hits, and the clean hits is listed in the table. The total number of all libraries in each column is plotted above the table. The percentage of potential hits and clean hits is in the parenthesis. The potential hits are screened compounds that have a minimum of 30% inhibitory effect at 10 μmol/L and the clean hits are those potential hits that are not cytotoxic or luciferase inhibitors.

Anti–c-Myc efficacy of nitazoxanide in cell culture

We first determined the IC_{50} of nitazoxanide *in vitro* using the SK-ST sensor stable cells and the SK-FST firefly luciferase stable cells as a control for direct inhibitory effect on luciferase activity. Nitazoxanide induced a dose-dependent reduction of sensor signals in SK-ST cells after 16 hours of treatment, whereas no significant changes occurred in SK-FST cells (Fig. 2A and B). The IC_{50} for the sensor signal inhibition of nitazoxanide was about 100 nmol/L, which was about 2,000- and 500-fold lower than that of c-Myc upstream kinase inhibitors, PD98059 and

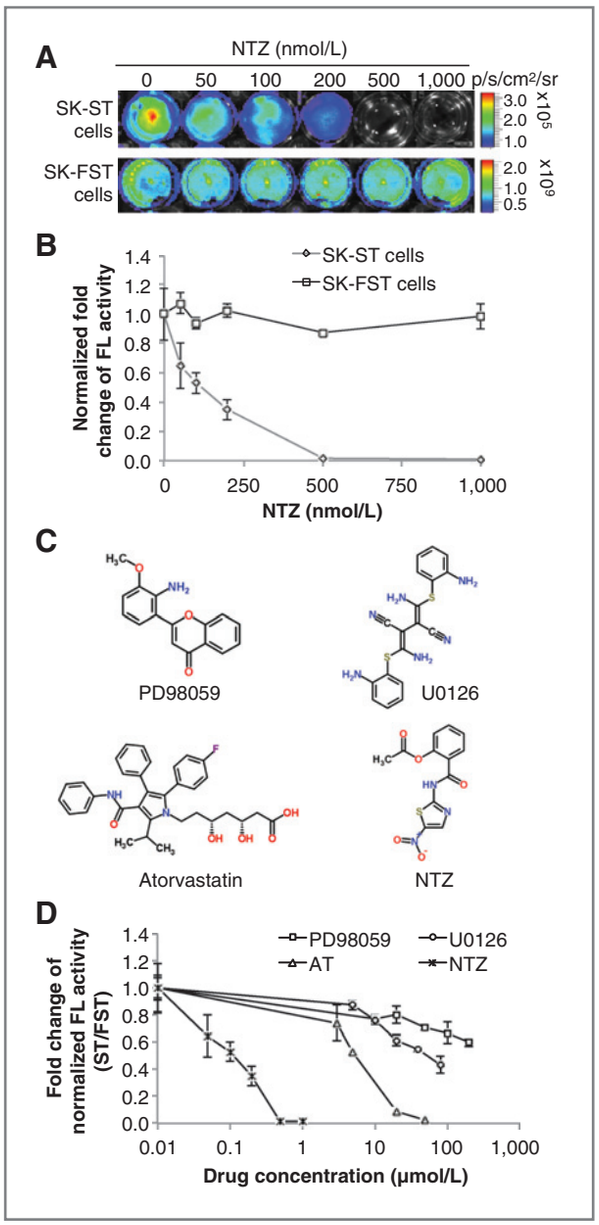

Figure 2. Efficacy of nitazoxanide (NTZ) in cell culture. A, SK-ST and SK-FST stable cells were treated with nitazoxanide at indicated concentrations and subjected to BLI as described in the Materials and Methods. B, plot of the fold change of firefly luciferase activity after normalization to cell numbers at different concentrations of nitazoxanide in SK-ST and SK-FST cells. C, the chemical structure of nitazoxanide and other three c-Myc inhibitors, PD98059, U0126, and atorvastatin. D, SK-ST and SK-FST cells were treated with indicated compounds at different concentrations (refer to Materials and Methods). Firefly luciferase activity of the SK-ST cells was normalized to that of the SK-FST cells and the fold change of the normalized firefly luciferase activity was plotted against the compound concentration.

U0126 (2), respectively (Fig. 2C and D), and about 50-fold lower than that for a HMG-coA inhibitor, atorvastatin, which was recently found to be a potent c-Myc inhibitor (3, 21). Moreover, nitazoxanide indeed induced a dose-dependent reduction of the endogenous phospho c-Myc and c-Myc proteins and the IC_{50} was consistent with that for the sensor signal (Fig. 3A). To examine the inhibitory spectrum of nitazoxanide, we also tested its efficacy in other c-Myc–associated tumor cell lines, lymphoma, and osteosarcoma cells. Nitazoxanide induced a dose-dependent reduction of the endogenous phospho c-Myc and c-Myc proteins in both cell lines (Supplementary Fig. S9A and S9B), with an IC_{50} of 440 nmol/L for lymphoma cells and 12 nmol/L for osteosarcoma cells (Fig. 3B). These results revealed a potent efficacy of nitazoxanide in c-Myc inhibition in different c-Myc–associated cancer cells. Furthermore, inhibition of c-Myc at nanomolar range of nitazoxanide resulted in slow cell growth rather than complete cell death. To determine the dose range of nitazoxanide for cell toxicity, we conducted a MTS assay in SKBR3 cells and determined that the half-maximal lethal dose (LD_{50}) of nitazoxanide was about 1 μmol/L (Supplementary Fig. S10), which was about 10-fold higher than its IC_{50}. This wide range between LD_{50} and IC_{50} implies a safe therapeutic effect of nitazoxanide.

Antitumor efficacy of nitazoxanide in mouse tumor models

To determine whether nitazoxanide could affect tumor growth as a single agent *in vivo*, we tested it in two tumor

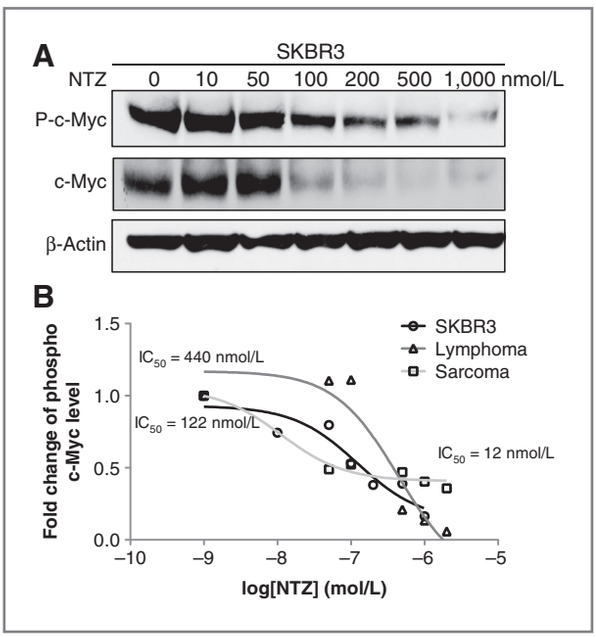

Figure 3. Inhibition of endogenous phosphorylation of c-Myc. A, Western blot analysis of SKBR3 cells after nitazoxanide (NTZ) treatment was conducted using phospho c-Myc, c-Myc protein, and β-actin antibodies. The blot of P-c-Myc was exposed overnight due to the weak signal under a short time exposure. Blots of c-Myc and β-Actin were exposed for 10 minutes and 2 seconds, respectively. B, nitazoxanide induced a dose-dependent inhibition of phospho c-Myc level in all three tumor cell lines, SKBR3 (IC_{50} = 122 nmol/L), lymphoma (IC_{50} = 440 nmol/L), and sarcoma cells (IC_{50} = 12 nmol/L). The fold change of phospho c-Myc level was plotted against the log scale of nitazoxanide concentration.

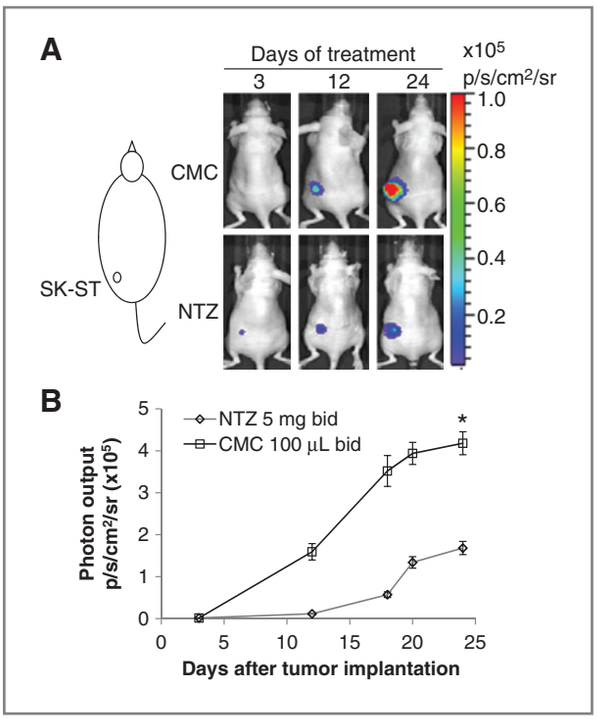

Figure 4. Efficacy of nitazoxanide (NTZ) in a breast cancer xenograft mouse model. A, SK-ST stable cells were subcutaneously implanted as indicated and treated with nitazoxanide or CMC as described in the Materials and Methods. Representative images of firefly luciferase imaging at indicated days of treatment are shown. B, photon output of SK-ST cells with nitazoxanide or CMC treatment is plotted against days after implantation. *, $P < 0.05$; bid, twice a day.

xenograft models. In one model, SK-ST cells were implanted subcutaneously into nude mice ($N = 12$; Fig. 4A) to monitor the effect of nitazoxanide on c-Myc activation, and in the other model, SK-FST cells were implanted ($N = 12$; Supplementary Fig. S11) to monitor cell numbers and the direct drug effect on firefly luciferase activity. Because there has not been any *in vivo* study on effective dosage of nitazoxanide in treating tumors, we chose a dose commonly used in animal models of protozoan infection that induces maximum growth inhibition without significant side effects (27, 28). Three days after implantation, mice were gavaged with nitazoxanide (200 mg/kg; $N = 6$) in 100 µL 0.5% CMC suspension or with the same volume of 0.5% CMC solution ($N = 6$) twice a day for 27 days. The same regimen was repeated three times for each model. We found that the bioluminescent signal from SK-ST xenografts increased rapidly 10 days after implantation in the CMC group, but is greatly inhibited in the nitazoxanide group (Fig. 4A and B). The signal of SK-FST xenografts slowly increased in both groups at the start, and about 18 days after implantation significant increase ($P < 0.05$) of the signal was seen in the CMC group, whereas sustained decrease of the signal was seen in the nitazoxanide group (Supplementary Fig. S11). This signal change was consistent with the change in tumor size, where 18 days after implantation the average tumor size of the CMC group was significantly larger ($P < 0.001$) than that of the nitazoxanide group (Fig. 5). Twenty-seven days after implantation in a SK-ST xenograft model, we dissected out tumors from each group and observed drastic inhibition of tumor growth in the nitazoxanide group by gross inspection and caliper measurements ($P = 0.00007$; Fig. 5A and B). H&E and Ki67 staining of the tumor samples indicated similar histology and cell proliferation pattern in the CMC and nitazoxanide groups. However, the caspase-3 staining in the nitazoxanide group gave average 23 ± 8 positive cells in each sample (Fig. 6A), which is significantly greater than the average 5 ± 2 positive cells in the CMC group ($P < 0.03$). This indicates that there is a significant increase of apoptosis in the nitazoxanide-treated group. The endogenous phospho and c-Myc protein levels were also greatly reduced in the tumor samples from the nitazoxanide group as compared with the CMC group (Fig. 6B). With this regimen, we did not observe the common side effects of nitazoxanide in animal models of protozoan infection, such as diarrhea, vomiting, and skin rash (7, 10). However, the mice had a 7% to 10% body weight loss in the nitazoxanide group but not in the CMC group 12 days after the implantation (Supplementary Fig. S12). This weight loss can be reversed upon removal of the nitazoxanide treatment. Together, these results showed an *in vivo* efficacy of nitazoxanide in inhibiting c-Myc activity and tumor growth.

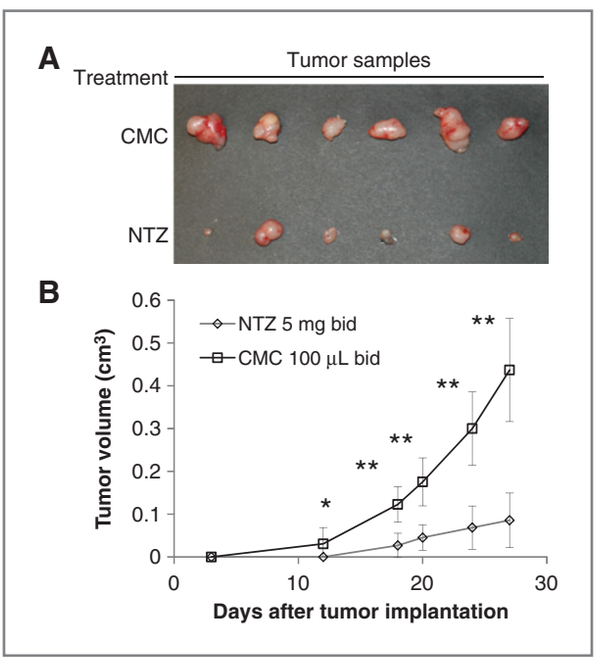

Figure 5. Inhibition of tumor growth by nitazoxanide (NTZ). A, representative photographs of dissected tumors from SK-ST xenograft mouse model with CMC or nitazoxanide treatment 27 days after implantation. B, plot of caliper-measured tumor sizes of nitazoxanide- or CMC-treated groups in SK-ST xenograft mouse model at different days after implantation. *, $P < 0.05$; **, $P < 0.01$; bid, twice a day.

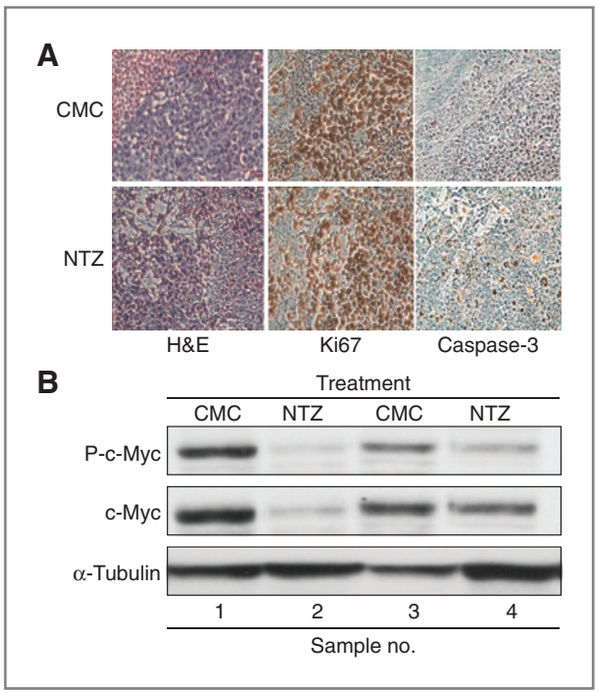

Figure 6. Immunohistochemistry and Western blot analysis of nitazoxanide (NTZ)-treated tumor samples. A, representative images of H&E, Ki67, and caspase-3 IHC staining of tumor tissue samples from each group. B, Western blot analysis of tumor tissue samples using phospho c-Myc, c-Myc, and α-tubulin antibodies.

Discussion

Deregulation of c-Myc at the transcriptional level involves mutation, translocation, and amplification of the *myc* gene, which makes targeting c-Myc at the gene expression level not an easy task. Regulation of c-Myc activity at the protein level is an attractive approach, but it is often indirect, as the protein lacks a clear ligand-binding domain for direct interaction (9). Thus, an effective targeting of c-Myc protein requires good understanding of its signaling pathways and regulation networks. However, there are currently more than 700 binary interactions of c-Myc according to the EBI IntAct, a comprehensive molecular interaction database, whereas new interactions keep adding to the list (10). Therefore, to identify an effective indirect target out of its complex network by examining the effect of each interaction is clearly labor intensive and often misses the network effect. Systematic profiling of drug-inhibitory effect on c-Myc not only can help identify inhibitors of a specific interaction but also discover unexpected multiple or cross-interactions, which in turn could reveal unknown function and molecular mechanisms involved in c-Myc signaling. Furthermore, profiling existing drugs for new use has become a more cost effective approach (29).

Efficient and large-scale profiling of compound libraries is enabled by HTS technology and a sensitive *in vitro* assay that can detect the target activity in a HTS format (30). We recently developed a c-Myc activation reporter system that is sensitive to compound inhibition-induced changes in c-Myc activity and allows rapid and quantitative detection of those changes in both intact cells and living mice (16). To facilitate systematic compound screening against c-Myc, we further developed this reporter system into a robust cell-based assay and optimized it in a HTS platform (Supplementary Figs. S1–S4). This new HTS system enables large-scale screening for compounds that regulate c-Myc activation in live cells. Furthermore, as the sensor-based assay measures changes at the level of the protein itself, it can capture upstream effects on c-Myc from both immediate and multilevel cross-interactions. Therefore, the targets of the resulted hits can be direct or indirect regulators of c-Myc activation. Although further low-throughput biologic assays are needed to examine the c-Myc activation-induced downstream effect, this system screens for upstream effectors and tends to identify more potent agents that potentially impact many downstream pathways of c-Myc rather than look for downstream effectors that only involve in a single or a few pathways.

We applied this new screening system on a qHTS platform and screened against 5 different libraries of about 5,000 compounds with known bioactivities. The qHTS platform allows compounds to be tested simultaneously in seven different concentrations. It not only facilitates rapid fitting and classification of the concentration–response curves for identification of compounds with a variety of potencies and efficacies, but also is more reliable than traditional single-concentration HTS due to the lower prevalence of false-negative hits (30). Not surprisingly, among all the clean hits antineoplastic compounds are the most frequently occurred. Interestingly, the second most frequently occurred are antiparasitic and antibacterial compounds (Supplementary Fig. S5). Nitazoxanide, one of the antiparasitic drugs, was among the top potent hits (Supplementary Fig. S6).

Nitazoxanide is a thiazolide (Fig. 2C) that consists of a nitrothiazole moiety (left) and a salicylic acid moiety (right) linked via a peptide bond (middle). Studies in different disease models suggest that different sites on nitazoxanide exert different functional activities. The nitro group in the nitrothiazole moiety is responsible for the activities against extracellular parasites and could be converted into a free radical that leads to cell death or interference in cell signaling pathways (31). The nitro group is also required for the inhibition of pyruvate ferredoxin oxidoreductase (PFOR) in anaerobic bacteria (32). The salicylic acid moiety, on the other hand, is responsible for the activities against intracellular parasites by interacting with thiazolide-binding proteins. More recent studies in other pathogens indicate that nitazoxanide has a broad-spectrum of activity by interfering in various signaling pathways. Studies in Hepatitis C suggested that nitazoxanide exhibits antiviral activity by inducing PKR (protein kinase activated by double-stranded RNA)-mediated phosphorylation of eIF2α that

enhances host cell antiviral defenses (33). A study in *Mycobacteria tuberculosis* suggests that nitazoxanide inhibits mTORC1 signaling pathway (34), which is known to regulate c-Myc activity. Another study in mouse macrophages showed inhibitory activity of nitazoxanide against interleukin-6 (IL-6) production (35). Although there was no reported *in vivo* study on antineoplastic activity of nitazoxanide, an *in vitro* study in human colon cancer cells suggested that nitazoxanide inhibits tumor cell growth by interaction with glutathione-S-transferase P1 (GSTP1; ref. 36). Interestingly, colon cancer has the highest *myc* overexpression among all human cancers (GenAtlas.org) and GSTP1 interferes the kinase activity of MAPK8 (37), which is an upstream regulator of c-Myc. Thus, the growth inhibition by nitazoxanide in colon cancer cells could be a downstream effect of c-Myc inhibition. Our study, for the first time, revealed a potent efficacy of nitazoxanide in c-Myc inhibition both in tumor cell lines and mouse tumor xenograft models.

To further explore the molecular mechanism of nitazoxanide's inhibitory effect on c-Myc, we first checked ChEMBL, a comprehensive bioactivity database for medicinal chemicals, and collected all experimentally identified nitazoxanide targets. There are total 30 different human targets of nitazoxanide, including MAPK1/ERK and TP53/P53 (Supplementary Fig. S13). Extracellular signal–regulated kinase (ERK) is the immediate upstream kinase of c-Myc, which phosphorylates and activates c-Myc, whereas the tumor suppressor protein P53 is often suppressed when c-Myc is activated. These *in vitro* data suggest potential pathways that nitazoxanide acts on to inhibit c-Myc activation. Because both ERK and TP53 act upstream of c-Myc activation, these data also provide validation for our screening strategy for upstream inhibitors of c-Myc. Alternatively, we found another antiparasitic family member, pyrvinium, has similar antineoplastic effect. It was shown that pyrvinium inhibits the cell growth of human colon cancer (38). Casien kinase 1α (CK1α) was identified as the target of pyrvinium. Interestingly, one of CK1α's targets, tau (39), is also a target of nitazoxanide (Supplementary Fig. S13).

The wide spectrum of nitazoxanide targets implies the complexity of its action. Nitazoxanide is supposed to bind its target to exert its function inside cells. Because c-Myc lacks a clear ligand-binding domain for direct interaction (40), nitazoxanide most likely affects c-Myc activity indirectly, and possibly via multiple routes. Further experiments to elucidate the molecular mechanism include examining upstream regulatory factors of c-Myc, such as the MAPK signaling pathway (Supplementary Fig. S13); c-Myc interacting cofactors, such as Max; or those indirect regulators, such as HMG-coA or eIF2α. A more systematic approach toward mechanistic determination might include obtaining a gene expression profile of nitazoxanide treatment using microarray analysis. Besides looking for alteration of gene expression of upstream regulators, this approach may also reveal expression profiles of downstream target genes and help pinpoint the effectors for nitazoxanide-induced apoptosis (Fig. 6A). More validation experiments for the antitumor efficacy of nitazoxanide would include applying nitazoxanide to various human cancer cell lines and tumor models, such as orthotopic or *in situ* conditional transgenic models (41). All these would help determine the spectrum of nitazoxanide efficacy against human cancers.

Further to its wide spectrum of activity, nitazoxanide is extremely well tolerated. It was the first antiparasitic compound developed for human use back in the mid-1990s (42) and is the only antiprotozoal drug approved for use in children. Indeed, there was a wide range between LD_{50} and EC_{50} of nitazoxanide in SKBR3 breast cancer cells (Fig. 3 and Supplementary Fig. S10). The ratio between LD_{50} and IC_{50} is often referred as the therapeutic index of the drug (43) and the higher the ratio the safer the drug. Our study indicates that at the effective dose, nitazoxanide inhibits c-Myc activation and induces apoptosis, thus inhibits tumor growth *in vivo* mouse model, rather than bluntly kills cell. The safe pharmaceutical profile of nitazoxanide for treatment of parasitic infections will likely help accelerate evaluation in any potential future clinical trials. Indeed, phase II clinical trials of nitazoxanide antiviral therapy were carried out before the understanding of its molecular mechanism of antiviral activity (44). These trials provided valuable information about effective regimens that cannot be obtained in preclinical experiments. For example, the realization that a 4-week lead-in of nitazoxanide monotherapy followed by combination therapy with a current anti-HCV agent provides sustained antiviral efficacy (45). The combination approach in antiviral therapy hints at the possible application of nitazoxanide in antineoplastic therapy. In fact, most of the top hits from our screen were antineoplastic agents (Supplementary Fig. S4), such as fludarabine phosphate (F-ara-A; Supplementary Fig. S8) currently used for chronic lymphocytic leukemia (CLL). Although it is interesting to figure out how a DNA analog has anti–c-Myc activity, it remains potentially of benefit to know whether combining F-ara-A and nitazoxanide could improve clinical outcome of CLL.

Here, we developed a new molecular imaging–based qHTS approach. By using it, we identified an anti–c-Myc effect of nitazoxanide and validated its efficacy in both tumor cell lines and mouse xenograft models. Our study provides evidence for a potential new spectrum of clinical applications of nitazoxanide. Moreover, the molecular imaging strategy coupled with systematic profiling of compound libraries promises to accelerate identification of new therapeutic agents or repurposing of known drugs, as well as their *in vivo* validation in preclinical models of disease.

Disclosure of Potential Conflicts of Interest

No potential conflicts of interest were disclosed.

Authors' Contributions

Conception and design: H. Fan-Minogue, A. Fan, R. Paulmurugan, T.F. Massoud, S.S. Gambhir

Development of methodology: H. Fan-Minogue, S. Bodapati, R. Paulmurugan, S.S. Gambhir
Acquisition of data (provided animals, acquired and managed patients, provided facilities, etc.): H. Fan-Minogue, D. Solow-Cordero, D. Felsher
Analysis and interpretation of data (e.g., statistical analysis, biostatistics, computational analysis): H. Fan-Minogue, S. Bodapati, D. Solow-Cordero, A. Fan, R. Paulmurugan, S.S. Gambhir
Writing, review, and/or revision of the manuscript: H. Fan-Minogue, A. Fan, R. Paulmurugan, T.F. Massoud, D. Felsher, S.S. Gambhir
Administrative, technical, or material support (i.e., reporting or organizing data, constructing databases): H. Fan-Minogue, S. Bodapati
Study supervision: T.F. Massoud, S.S. Gambhir

Acknowledgments

The authors thank Dr. Carmel Chan for critical review and suggestions.

Grant Support

This work is supported in part by National Cancer Institute grants, R01 CA82214 (to S.S. Gambhir) and ICMIC P50 CA114747 (to S.S. Gambhir). H. Fan-Minogue is supported by a NIH R25T CA118681 training grant. T.F. Massoud received partial salary support from the National Institute of Health Research (NIHR) Cambridge Biomedical Research Center.

The costs of publication of this article were defrayed in part by the payment of page charges. This article must therefore be hereby marked *advertisement* in accordance with 18 U.S.C. Section 1734 solely to indicate this fact.

Received January 8, 2013; revised May 28, 2013; accepted June 18, 2013; published OnlineFirst July 3, 2013.

References

1. Beroukhim R, Mermel CH, Porter D, Wei G, Raychaudhuri S, Donovan J, et al. The landscape of somatic copy-number alteration across human cancers. Nature 2010;463:899–905.
2. Eilers M, Eisenman RN. Myc's broad reach. Genes Dev 2008;22:2755–66.
3. Jain M, Arvanitis C, Chu K, Dewey W, Leonhardt E, Trinh M, et al. Sustained loss of a neoplastic phenotype by brief inactivation of MYC. Science 2002;297:102–4.
4. Soucek L, Whitfield J, Martins CP, Finch AJ, Murphy DJ, Sodir NM, et al. Modelling Myc inhibition as a cancer therapy. Nature 2008;455:679–83.
5. Hermeking H. The MYC oncogene as a cancer drug target. Curr Cancer Drug Targets 2003;3:163–75.
6. Wang YH, Liu S, Zhang G, Zhou CQ, Zhu HX, Zhou XB, et al. Knockdown of c-Myc expression by RNAi inhibits MCF-7 breast tumor cells growth *in vitro* and *in vivo*. Breast Cancer Res 2005;7:R220–8.
7. Kim HG, Miller DM. Inhibition of *in vitro* transcription by a triplex-forming oligonucleotide targeted to human c-myc P2 promoter. Biochemistry 1995;34:8165–71.
8. Kimura S, Maekawa T, Hirakawa K, Murakami A, Abe T. Alterations of c-myc expression by antisense oligodeoxynucleotides enhance the induction of apoptosis in HL-60 cells. Cancer Res 1995;55:1379–84.
9. Vita M, Henriksson M. The Myc oncoprotein as a therapeutic target for human cancer. Semin Cancer Biol 2006;16:318–30.
10. Delmore JE, Issa GC, Lemieux ME, Rahl PB, Shi J, Jacobs HM, et al. BET bromodomain inhibition as a therapeutic strategy to target c-Myc. Cell 2011;146:904–17.
11. Dawson MA, Prinjha RK, Dittmann A, Giotopoulos G, Bantscheff M, Chan WI, et al. Inhibition of BET recruitment to chromatin as an effective treatment for MLL-fusion leukaemia. Nature 2011;478:529–33.
12. Berg T, Cohen SB, Desharnais J, Sonderegger C, Maslyar DJ, Goldberg J, et al. Small-molecule antagonists of Myc/Max dimerization inhibit Myc-induced transformation of chicken embryo fibroblasts. Proc Natl Acad Sci U S A 2002;99:3830–5.
13. Mo H, Henriksson M. Identification of small molecules that induce apoptosis in a Myc-dependent manner and inhibit Myc-driven transformation. Proc Natl Acad Sci U S A 2006;103:6344–9.
14. Hydbring P, Bahram F, Su Y, Tronnersjo S, Hogstrand K, von der Lehr N, et al. Phosphorylation by Cdk2 is required for Myc to repress Ras-induced senescence in cotransformation. Proc Natl Acad Sci U S A 2009;107:58–63.
15. Fremin C, Meloche S. From basic research to clinical development of MEK1/2 inhibitors for cancer therapy. J Hematol Oncol 2010;3:8.
16. Fan-Minogue H, Cao Z, Paulmurugan R, Chan CT, Massoud TF, Felsher DW, et al. Noninvasive molecular imaging of c-Myc activation in living mice. Proc Natl Acad Sci U S A 2010;107:15892–7.
17. Cao Z, Fan-Minogue H, Bellovin DI, Yevtodiyenko A, Arzeno J, Yang Q, et al. MYC phosphorylation, activation, and tumorigenic potential in hepatocellular carcinoma are regulated by HMG-CoA reductase. Cancer Res 2011;71:2286–97.
18. Willmann JK, van Bruggen N, Dinkelborg LM, Gambhir SS. Molecular imaging in drug development. Nat Rev Drug Discov 2008;7:591–607.
19. Tseng JR, Stuart D, Aardalen K, Kaplan A, Aziz N, Hughes NP, et al. Use of DNA microarray and small animal positron emission tomography in preclinical drug evaluation of RAF265, a novel B-Raf/VEGFR-2 inhibitor. Neoplasia 2011;13:266–75.
20. Chan CT, Paulmurugan R, Gheysens OS, Kim J, Chiosis G, Gambhir SS. Molecular imaging of the efficacy of heat shock protein 90 inhibitors in living subjects. Cancer Res 2008;68:216–26.
21. Fukazawa T, Maeda Y, Matsuoka J, Yamatsuji T, Shigemitsu K, Morita I, et al. Inhibition of Myc effectively targets KRAS mutation-positive lung cancer expressing high levels of Myc. Anticancer Res 2010;30:4193–200.
22. Zhang JH, Chung TD, Oldenburg KR. A simple statistical parameter for use in evaluation and validation of high throughput screening assays. J Biomol Screen 1999;4:67–73.
23. Sigma-Aldrich. LOPAC$^{1280_{TM}}$: a versatile library for assay validation and high throughput screening. Sigma Product Assets 2004.
24. Kaneto H, Suzuma K, Sharma A, Bonner-Weir S, King GL, Weir GC. Involvement of protein kinase C beta 2 in c-myc induction by high glucose in pancreatic beta-cells. J Biol Chem 2002;277:3680–5.
25. Kobayashi E, Nakano H, Morimoto M, Tamaoki T. Calphostin C (UCN-1028C), a novel microbial compound, is a highly potent and specific inhibitor of protein kinase C. Biochem Biophys Res Commun 1989;159:548–53.
26. White CA Jr. Nitazoxanide: a new broad spectrum antiparasitic agent. Expert Rev Anti Infect Ther 2004;2:43–9.
27. Zhao Z, Xue F, Zhang L, Zhang K, Fei C, Zheng W, et al. The pharmacokinetics of nitazoxanide active metabolite (tizoxanide) in goats and its protein binding ability *in vitro*. J Vet Pharmacol Ther 2010;33:147–53.
28. Theodos CM, Griffiths JK, D'Onfro J, Fairfield A, Tzipori S. Efficacy of nitazoxanide against Cryptosporidium parvum in cell culture and in animal models. Antimicrob Agents Chemother 1998;42:1959–65.
29. Harrison C. Signatures for drug repositioning. Nat Rev Genet 2011;12:668.
30. Inglese J, Auld DS, Jadhav A, Johnson RL, Simeonov A, Yasgar A, et al. Quantitative high-throughput screening: a titration-based approach that efficiently identifies biological activities in large chemical libraries. Proc Natl Acad Sci U S A 2006;103:11473–8.
31. Hemphill A, Mueller J, Esposito M. Nitazoxanide, a broad-spectrum thiazolide anti-infective agent for the treatment of gastrointestinal infections. Expert Opin Pharmacother 2006;7:953–64.
32. Sisson G, Goodwin A, Raudonikiene A, Hughes NJ, Mukhopadhyay AK, Berg DE, et al. Enzymes associated with reductive activation and action of nitazoxanide, nitrofurans, and metronidazole in Helicobacter pylori. Antimicrob Agents Chemother 2002;46:2116–23.
33. Elazar M, Liu M, McKenna SA, Liu P, Gehrig EA, Puglisi JD, et al. The anti-hepatitis C agent nitazoxanide induces phosphorylation of eukaryotic initiation factor 2alpha via protein kinase activated by double-stranded RNA activation. Gastroenterology 2009;137:1827–35.
34. Lam KK, Zheng X, Forestieri R, Balgi AD, Nodwell M, Vollett S, et al. Nitazoxanide stimulates autophagy and inhibits mTORC1 signaling

and intracellular proliferation of Mycobacterium tuberculosis. PLoS Pathog 2012;8:e1002691.
35. Hong SK, Kim HJ, Song CS, Choi IS, Lee JB, Park SY. Nitazoxanide suppresses IL-6 production in LPS-stimulated mouse macrophages and TG-injected mice. Int Immunopharmacol 2012;13:23–7.
36. Muller J, Sidler D, Nachbur U, Wastling J, Brunner T, Hemphill A. Thiazolides inhibit growth and induce glutathione-S-transferase Pi (GSTP1)-dependent cell death in human colon cancer cells. Int J Cancer 2008;123:1797–806.
37. Elsby R, Kitteringham NR, Goldring CE, Lovatt CA, Chamberlain M, Henderson CJ, et al. Increased constitutive c-Jun N-terminal kinase signaling in mice lacking glutathione S-transferase Pi. J Biol Chem 2003;278:22243–9.
38. Thorne CA, Hanson AJ, Schneider J, Tahinci E, Orton D, Cselenyi CS, et al. Small-molecule inhibition of Wnt signaling through activation of casein kinase 1alpha. Nat Chem Biol 2010;6:829–36.
39. Gao ZH, Seeling JM, Hill V, Yochum A, Virshup DM. Casein kinase I phosphorylates and destabilizes the beta-catenin degradation complex. Proc Natl Acad Sci U S A 2002;99:1182–7.
40. Darnell JE Jr. Transcription factors as targets for cancer therapy. Nat Rev Cancer 2002;2:740–9.
41. Guttner Y, Windsor HM, Viiala CH, Dusci L, Marshall BJ. Nitazoxanide in treatment of Helicobacter pylori: a clinical and *in vitro* study. Antimicrob Agents Chemother 2003;47:3780–3.
42. Fox LM, Saravolatz LD. Nitazoxanide: a new thiazolide antiparasitic agent. Clin Infect Dis 2005;40:1173–80.
43. Stanley TH. Anesthesia for the 21st century. Proc (Bayl Univ Med Cent) 2000;13:7–10.
44. Rossignol JF, Kabil SM, El-Gohary Y, Elfert A, Keeffe EB. Clinical trial: randomized, double-blind, placebo-controlled study of nitazoxanide monotherapy for the treatment of patients with chronic hepatitis C genotype 4. Aliment Pharmacol Ther 2008;28:574–80.
45. Rossignol JF, Elfert A, Keeffe EB. Treatment of chronic hepatitis C using a 4-week lead-in with nitazoxanide before peginterferon plus nitazoxanide. J Clin Gastroenterol 2010;44:504–9.